

Theoretical study of the alignment-to-orientation conversion in magneto-optical rotation based on atomic multipole moments

Pan-li Qi ¹, Xu-xing Geng ¹, Guo-qing Yang², Shao-ping Wu,¹ Guang-ming Huang,^{1,*} and Gao-xiang Li ^{1,†}

¹Department of Physics, Huazhong Normal University, Wuhan 430079, China

²College of Electronics and Information, Hangzhou Dianzi University, Hangzhou 310018, China



(Received 10 August 2021; accepted 16 March 2022; published 29 March 2022)

We theoretically investigate the magneto-optical rotation (MOR) effect in cesium atoms in the Voigt geometry, in which an off-resonance linearly polarized laser beam serves as both pump and probe. By calculating the detailed evolution of atomic multipole moments truncated to second-rank, alignment-to-orientation conversion (AOC) effects are observed in two hyperfine ground states. The mechanisms responsible for this effect are demonstrated. The tensor AC-Stark shift produced by the optical pumping generates a nonlinear effect, resulting in atomic alignment directly coupled to orientation, which enables spin orientation to be obtained. Simultaneously, spin-exchange collisions lead to atomic alignment and orientation transfer between two ground-state manifolds. Additionally, we present the analytical expression of atomic spin polarization described by atomic multipole moments, and the contributions of the AOC effect to the optical-rotation signals are discussed in different light power regimes. Our results can be helpful for guiding MOR experiments by refining and optimizing the parameters.

DOI: [10.1103/PhysRevA.105.033112](https://doi.org/10.1103/PhysRevA.105.033112)

I. INTRODUCTION

The magneto-optical rotation (MOR) effect is the rotation of an optical field's polarization as the light propagates through a medium in the presence of an applied magnetic field [1–3]. The most prominent magneto-optical effects are the Faraday [4] effect and Voigt effect [5], which depend on the longitudinal and transverse orientations of the external magnetic field, respectively, with respect to the propagation direction of the light field. Numerous theoretical and experimental studies have been reported on the MOR of the polarization plane in various wavelength regions in atomic gasses [6–8], GaAs quantum well waveguide [9], metamaterials [10], graphene [11,12], and nitrogen-vacancy centers [13]. The signals of optical rotation and ellipticity in MOR experiments have a wide variety of applications in electron-dipole-moment measurements [14], atomic clocks [15], and sensitive magnetometry [16–18].

In atomic systems, the focus of the MOR is to investigate the generation and coherent control of atomic spin polarization with the combined action of the magnetic field and optical field [19–21]. In general, the coherence properties of atomic states can be described by the notions of “orientation” and “alignment” [20]. An atomic state is said to be oriented along some axis if the magnetic sublevels associated with the quantum number M and $-M$ have different populations. Similarly, we say that the state is aligned if the sublevels with different values of $|M|$ have different populations. Traditionally, atomic spin orientation or alignment is achieved

by the transfer of angular momentum from polarized light to an atomic system. However, the atomic alignment created by linear-polarized light can be converted to orientation by external interactions such as a magnetic field gradient [22], anisotropic collisions [23], or the AC-Stark shift induced by optical pumping [24–26]. This process is known as alignment-to-orientation conversion (AOC) [27].

The AOC is an important mechanism for atomic magnetometry and has been extensively studied for many years, both theoretically and experimentally. Budker *et al.* [28] have considered the AOC in nonlinear magneto-optical rotation (NMOR), which causes optical rotation via circular birefringence. They also demonstrated that the AOC occurring in nuclear quadrupole resonance (NQR) is the mechanism responsible for the appearance of macroscopic orientation in a sample originally lacking any global polarization [29]. A close relationship between AOC and spin squeezing has been demonstrated [30]. Recently, to illustrate the AOC effect, the detailed mechanism of the generation of spin orientation in room-temperature cesium vapor has been explored in Ref. [31]. This combines three elements: (i) off-resonant optical pumping, (ii) nonlinear spin dynamics generated by a linearly polarized probe beam [32], and (iii) spin-exchange collision (SEC).

Although the AOC effect has been theoretically investigated using density-matrix theory for various alkali-metal atoms in previous studies [28,30], it is not easy to explicitly explain the physical mechanisms of the AOC effect, especially in specific alkali-metal atoms with multipole levels. In order to better understand the mechanisms responsible for the AOC effect and further simplify the analytical expression of optical rotation signals, we present a theoretical study of the MOR effect using atomic multiple-moment theory [33]. The

*gmhuang@mail.ccnu.edu.cn

†gaox@mail.ccnu.edu.cn

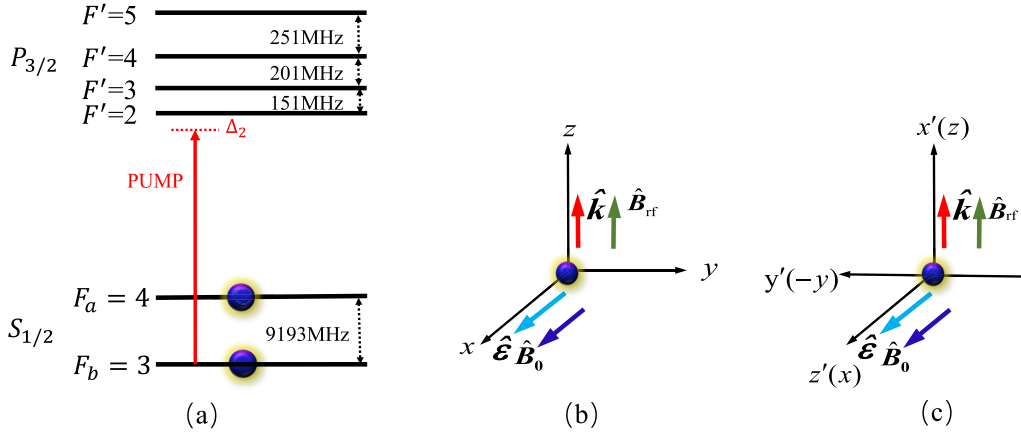


FIG. 1. (a) Energy structure of the cesium $6^2S_{1/2} \rightarrow 6^2P_{3/2}$ transition (D_2 line, 852 nm). The atomic ensemble is optically pumped by a linearly polarized laser beam, frequency locked close to $F_b = 3 \rightarrow F' = 2$ of cesium D_2 line (red-dashed arrow in level scheme). (b) Laboratory-frame xyz , referred to as the laboratory frame: the quantization axis is along the light propagation direction z and the light polarization axis is along x . An offset static magnetic field \mathbf{B}_0 is applied along x axis and a weak radio-frequency (rf) field \mathbf{B}_{rf} is along z axis. The same linearly polarized laser beam, acting as the probe, monitors the spin precession via the Voigt effect. (c) Rotation frame $x'y'z'$: described in a coordinate frame obtained from the laboratory-frame xyz by a static rotation of $\pi/2$ around the y axis and then by a rotation of π around the new z' axis. We choose the light polarization direction $z'(x)$ axis as the quantization axis.

Voigt geometry of cesium atoms considered in this paper is similar to that of in Refs. [31,32]. An off-resonance linearly polarized laser beam serves as both pump and probe, and atomic spin polarization is produced by parallel magnetic and laser fields. By calculating the detailed evolution of atomic multipole moments truncated to second-rank, we observe that the AOC effects appear in two ground-state manifolds [shown in Fig. 1(a)]. For the $F_b = 3$ state, which is directly coupled to the pump light, the tensor Stark shift Δ_{AC} produced by the optical pumping generates a nonlinear effect, resulting in atomic alignment directly coupled to orientation. Consequently, the conversion of alignment into orientation can be achieved. However, the $F_a = 4$ state is not coupled to light, the orientation of this state is achieved indirectly, as a consequence of a direct orientation of the $F_b = 3$ states and SEC. In addition, the degree of atomic orientation and its contribution to the optical-rotation signals are investigated under different light power regimes. For low light intensity, atomic alignment is observed in both ground states. As the tensor Stark shift is increased to satisfy $\delta_a = \delta_b + 3\Delta_{\text{AC}}$ (δ_a and δ_b are the detuning between the Larmor frequency of the F_a and F_b states and the Rabi frequency of the rf field), the coupling between two ground states induced by the SEC reaches maximum, equalizing population distribution in two ground states. In this case, the degree of spin orientation is comparable to that of alignment. In the regime of high light intensity, atomic orientation of $F_b = 3$ manifold is significantly larger than its alignment and dominates the MOR signals.

II. THEORETICAL MODEL OF MAGNETO-OPTICAL ROTATION

A. Theoretical model of magneto-optical rotation

The energy structure of the cesium $6^2S_{1/2} \rightarrow 6^2P_{3/2}$ transition (D_2 line, 852 nm) is shown in Fig. 1(a). A linearly polarized laser beam propagates along the z axis, frequency ω_L locked close to $F_b = 3 \rightarrow F' = 2$ transition, and the

detuning $\Delta_2 = \omega_{F_b F' = 2} - \omega_L$. Choosing the light propagation direction as the quantization axis, the light-atom interaction Hamiltonian is given by $H_L = -\mathbf{E} \cdot \mathbf{d} = -E_0 \cos(\omega_L t) d_x = -\frac{1}{\sqrt{2}} E_0 \cos(\omega_L t) (d_{-1} - d_{+1})$, where E_0 is the amplitude of the light field, \mathbf{d} is the dipole operator, and $d_q (q = 0, \pm 1)$ are these components in the spherical basis. According to the Wigner-Eckart theorem, [3], the matrix elements of d_q can be written as $\langle J F M_F | d_q | J' F' M'_F \rangle = V_{F M_F}^{F' M'_F} \langle J || \mathbf{d} || J' \rangle$. Coefficient $V_{F M_F}^{F' M'_F}$ is the transition coefficient between the ground state $|J F M_F\rangle$ and the excited state $|J' F' M'_F\rangle$, and the double bar indicates that the matrix element is reduced. Therefore, the reduced Rabi frequency of the pumping light is defined as $\Omega_L = -E_0 \langle J || \mathbf{d} || J' \rangle$. In our calculations we assume that the $F_b = 3$ state is directly coupled to the pump light, while the $F_a = 4$ state is not coupled to light (the 9193 MHz detuning of the light reduces the optical excitation).

In Fig. 1(b), a static magnetic field \mathbf{B}_0 , parallel to the light polarization vector, causes the linear Zeeman splitting of the magnetic sublevels. The Larmor frequencies of the two hyperfine ground states $F_a = 4$ and $F_b = 3$ are written as $\omega_a = \mu_B g_{F_a} B_0$ and $\omega_b = \mu_B g_{F_b} B_0$, respectively, where μ_B is the Bohr magneton, and g_{F_a} and g_{F_b} are the corresponding Landé g factors. Note that the two ground states show opposite precession directions and different g -factor values. The rf field \mathbf{B}_{rf} is directed orthogonally to the static magnetic field. One can derive the $\Delta M_F = \pm 1$ transitions between the ground-state Zeeman sublevels in the same manifold. The same linearly polarized laser beam, acting as the probe, monitors the spin precession via the Voigt effect, where the evolution of the collective atomic spin is mapped onto the polarization state of the linearly polarized probe beam. The rf transitions are monitored via rotation of the polarization plane of linearly polarized probe light. The difference in g factors of the $F_b = 3$ and $F_a = 4$ levels causes the rotation resonances to be detected at different rf frequencies.

B. Effect of atoms on transmitted light

It is well known that the changes in the electric field of a plane light wave as it traverses an atomic medium can be described in terms of the α - ϵ parametrization [3]. Thus the electric field \mathcal{E} of a plane wave of frequency ω with arbitrary polarization and \mathbf{z} propagation can be described by

$$\mathcal{E} = \text{Re} \{ \mathcal{E}_0 e^{i(kz - \omega t + \varphi)} [(\cos \alpha \cos \epsilon - i \sin \alpha \sin \epsilon) \hat{\mathbf{e}}_x + (\sin \alpha \cos \epsilon + i \cos \alpha \sin \epsilon) \hat{\mathbf{e}}_y] \}, \quad (1)$$

where \mathcal{E}_0 is amplitude of the electric field, φ is an overall phase, α is the polarization angle with respect to the $\hat{\mathbf{e}}_x$ axis, and ϵ is the ellipticity. As with this light field, the polarization of the medium \mathbf{P} can be written as

$$\mathbf{P} = \text{Re} \{ e^{i(kz - \omega t + \varphi)} [(P_1 - iP_2) \hat{\mathbf{e}}_x + (P_3 - iP_4) \hat{\mathbf{e}}_y] \}, \quad (2)$$

where P_i ($i = 1, 2, 3, 4$) are the in-phase and quadrature components of the polarization. The electric field \mathcal{E} and the polarization of the medium \mathbf{P} are connected by the wave equation

$$\left(\frac{d^2}{dz^2} - \frac{d^2}{c^2 dt^2} \right) \mathcal{E} = \frac{4\pi}{c^2} \frac{d^2}{dt^2} \mathbf{P}, \quad (3)$$

where z is the distance along the light propagation direction. Neglecting terms involving second-order derivatives and products of first-order derivatives, we can solve the wave equation to find expressions for the change of the light-field parameters per unit distance for initial values of $\alpha = \epsilon = 0$,

$$\frac{1}{\mathcal{E}_0} \frac{d\mathcal{E}_0}{dz} = \frac{2\pi\omega}{\mathcal{E}_0 c} P_2, \quad (4a)$$

$$\frac{d\varphi}{dz} = \frac{2\pi\omega}{\mathcal{E}_0 c} P_1, \quad (4b)$$

$$\frac{d\alpha}{dz} = \frac{2\pi\omega}{\mathcal{E}_0 c} P_4, \quad (4c)$$

$$\frac{d\epsilon}{dz} = \frac{2\pi\omega}{\mathcal{E}_0 c} P_3. \quad (4d)$$

C. Evolution equations of density-matrix elements

We are going to investigate the evolution equations of atoms in the Voigt geometry using density-matrix theory. For simplicity, it is convenient to choose the light polarization axis, which is also the direction of the static magnetic field, as the quantization axis. Therefore, our calculations are carried out in the rotation frame $x'y'z'$ shown in Fig. 1(c), which is obtained from the laboratory-frame xyz [Fig. 1(b)] by a static rotation of $\pi/2$ around the y axis and then by a rotation of π around the new z' axis.

In the Voigt geometry shown in Fig. 1, we assume the total spontaneous emission rate of the excited states $|F'\rangle$ to the two ground states $F_a = 4$ and $F_b = 3$ is much greater than the Rabi frequency of the light field. In this case, the time of the excited-state atoms evolving to a steady state is much less than that of the ground-state atoms, and the excited states can therefore be adiabatically eliminated. Consequently, the evolution of our system is governed by the effective master equations in the ground-state subspace. The effective Hamiltonian is the sum of the unperturbed Hamiltonian,

the light-atom-interaction Hamiltonian, and the magnetic-field-atom-interaction Hamiltonian. The detailed derivation is shown in Appendix A, and the effective Hamiltonian is given by

$$H_{\text{eff}} = \tilde{H}_0 + \Delta_{\text{AC}} (F_z^{(b)})^2 + \delta_a F_z^{(a)} - \delta_b F_z^{(b)} + \Omega_{\text{rf}} [(F_+^{(a)} + F_-^{(a)}) - (F_+^{(b)} + F_-^{(b)})]. \quad (5)$$

Here $\tilde{H}_0 = -\Delta \sum_{M_{F_b}} |F_b M_{F_b}\rangle \langle F_b M_{F_b}|$ represents the unperturbed Hamiltonian, where $\Delta = 9193$ MHz is the hyperfine detuning of two ground states. $F^{(a)}$ and $F^{(b)}$ are the angular momentum operators applied to the higher ground state $F_a = 4$ and the lower ground state $F_b = 3$, respectively.

The second term of Eq. (5) represents the tensor AC-Stark shift produced by the off-resonance linearly polarized light. The angular momentum operator $(F_z^{(b)})^2$ causes a nonlinear effect in the $F_b = 3$ ground-state Zeeman sublevels, therefore collective atomic spin dynamics will exhibit a nonlinear character. In general, the AC-Stark shift depends on the pumping field and the atomic tensor polarizability, and consists of scalar, vector, and rank-2 tensor components. However, in our system, the vector component is identically zero since the pump polarization is linear. We also neglect the scalar polarizability term and the part of the tensor polarizability that is independent of $F_z^{(b)}$ since they result only in a common shift of the Zeeman sublevels of the ground state $F_b = 3$. While the tensor Stark shifts cause different magnetic quantum number states to have different Stark shifts, and this can significantly affect the evolution of coherences among the atomic sublevels, thereby affecting the polarization of the light emitted (or absorbed) by those states. In our system, the expression of Δ_{AC} is given by

$$\Delta_{\text{AC}} = \Omega_L^2 \left(\frac{5}{168} \frac{2\Delta_4}{\Gamma^2 + 4\Delta_4^2} + \frac{2}{21} \frac{2\Delta_2}{\Gamma^2 + 4\Delta_2^2} - \frac{1}{8} \frac{2\Delta_3}{\Gamma^2 + 4\Delta_3^2} \right). \quad (6)$$

We see that the tensor AC-Stark shift not only depends on the Rabi frequency of light Ω_L and the total spontaneous emission rate Γ , but also on the detuning $\Delta_{F'} = \omega_{F',F'} - \omega_L$ between the atomic $F_b = 3 \rightarrow F'$ ($F' = 2, 3, 4$) transition frequency and the laser frequency. Here $\Delta_3 = \Delta_2 + 151$ MHz and $\Delta_4 = \Delta_2 + 352$ MHz.

The remaining terms of Eq. (5) represent the magnetic-field-atom interaction, involving the combined action of the offset magnetic field \mathbf{B}_0 and the rf field \mathbf{B}_{rf} . Here $\delta_a = \omega_a - \omega_{\text{rf}}$ and $\delta_b = \omega_b - \omega_{\text{rf}}$ are the detunings of the Larmor frequency ω_a and ω_b with respect to the rf frequency ω_{rf} , respectively. Due to the rf field is much weaker than the static magnetic field, the Rabi frequency of the rf field corresponding to two ground states can be assumed to be the same $\Omega_{\text{rf}} = 1/2 \mu_B |g_F| B_{\text{rf}}$.

Consequently, our ensemble of cesium atoms in the Voigt geometry can therefore be described by the 16×16 rotating-frame density matrix $\tilde{\rho}$ in the ground-state subspace, and the time evolution of $\tilde{\rho}$ is governed by the Liouville equation as

adapted from Ref. [2]:

$$\frac{d}{dt}\tilde{\rho} = -i[H_{\text{eff}}, \tilde{\rho}] + \mathcal{L}_L(\tilde{\rho}) - \frac{1}{2}\{R, \tilde{\rho}\} + \Lambda + \mathcal{L}_{\text{sc}}(\tilde{\rho}). \quad (7)$$

After adiabatically eliminating the excited states, the combined action of the optical pumping and spontaneous emission is equivalent to the combined action of the tensor AC-Stark effect and the laser-induced equivalent relaxation process $\mathcal{L}_L(\tilde{\rho})$, the detailed expression is given in Appendix A. The matrix R accounts for the uniform relaxation and depolarization of all atomic states due to effects such as wall- and buffer-gas collisions. The matrix Λ describes the repopulation of the ground-state Zeeman sublevels due to the uniform relaxation. The last term of Eq. (7) $\mathcal{L}_{\text{sc}}(\tilde{\rho})$ represents the spin-exchange collision relaxation, incorporating relaxation and repopulation due to spin-exchange collisions, and colliding ground-state atoms in different hyperfine Zeeman states exchange their quantum numbers such that $M_{F_a} + M_{F_b}$ is conserved [34].

D. Evolution equations of atomic multipole moments

In Sec. II C the evolution of the ensemble of cesium atoms in Voigt geometry has been described in Eq. (7). Similar density-matrix calculations have been investigated in previous studies [35,36]. However, the steady-state solutions of the 16×16 density-matrix equations are too cumbersome to solve. Therefore, in order to further simplify the analytical expression of MOR signals and better understand the mechanisms responsible for the AOC effect, we will present a theoretical study of the MOR signals from a new perspective by transferring the density matrix element $\tilde{\rho}$ to atomic multipole moments $m_{k,q}$ [33]. One can directly describe the spin polarization of the medium.

The transform between density matrix elements and atomic multipole moments obeys [33]

$$\rho = \sum_{k=0}^{2F} \sum_{q=-k}^k m_{k,q} T_{kq}, \quad (8)$$

where T_{kq} is irreducible tensor operator. The $m_{k,q}$ is irreducible component of atomic multipole moments. (1) The

tensor with rank $k = 0$ is merely a normalization constant. (2) The three components with $k = 1$ are often called orientation vector, and can be expressed in terms of quadratic combinations of the angular momentum components as $m_{1,q} = N_1 \langle F_q^\dagger \rangle \text{tr} \rho$. (3) The five components with $k = 2$ are often called the alignment tensor and obey $m_{2,0} = \frac{N_2}{\sqrt{6}} (3F_z^2 - F^2) \text{tr} \rho$, $m_{2,\pm 1} = \mp \frac{N_2}{2} (F_x F_z + F_z F_x) \text{tr} \rho$, and $m_{2,\pm 2} = \frac{N_2}{2} (F_x^2 - F_y^2) \text{tr} \rho$, where N_1 and N_2 are the constants related to the quantum number F . Moreover, the longitudinal multipole moments $m_{k,0}$ can be expressed as linear combinations of the sublevel populations $\rho_{M,M}$, and the transverse moments $m_{k,q \neq 0}$ are determined by the $\Delta M = q$ coherences $\rho_{M,M-q}$.

Substituting Eq. (7) into Eq. (8), the evolution equations of atomic multipole moments corresponding to two ground states are obtained. Note that since the hyperfine detuning Δ of two ground states is much larger than the Larmor frequency (both ω_a and ω_b), the off-diagonal matrix elements ρ_{M_a, M_b} are oscillating with the hyperfine frequency and average to zero. Under this approximation, our system are well derived by the evolution equations of full-rank atomic multipole moments $\{m_{k,q}^a (k = 0, 1, 2, \dots, 2F_a; q = -k \dots k), m_{k,q}^b (k = 0, 1, 2, \dots, 2F_b; q = -k \dots k)\}$, where $m_{k,q}^a$ and $m_{k,q}^b$ represent atomic multipole moments corresponding to the $F_a = 4$ and $F_b = 3$ manifolds, respectively.

For further simplicity, the contribution of atomic multipole moments higher than second-rank can be neglected when the laser-induced relaxation rate is much smaller than the SEC relaxation rate. This assumption has been demonstrated in many experimental and theoretical studies [37–39]. Therefore, the full-rank evolution equations of atomic multipole moments $\{m_{k,q}^a (k = 0, 1, 2, \dots, 2F_a; q = -k \dots k), m_{k,q}^b (k = 0, 1, 2, \dots, 2F_b; q = -k \dots k)\}$ can be truncated to second-rank, i.e., our system can be well described in the basis vectors $\{m_{k,q}^a, m_{k,q}^b\} (k = 0, 1, 2; q = -k \dots k)$.

We first focus on atomic multipole moments $m_{k,q}^b (k = 0, 1, 2; q = -k \dots k)$ of the $F_b = 3$ state, which is directly coupled to the pump light. The evolution equations of $m_{k,q}^b (k = 0, 1, 2; q = -k \dots k)$ are given by

$$\frac{d}{dt} m_{1,0}^b = -(c_1^b + p_{10}^b) m_{1,0}^b + \frac{\sqrt{2}}{2} i \Omega_{\text{rf}} (m_{1,1}^b + m_{1,-1}^b) + c_1^{\text{se}} m_{1,0}^a, \quad (9a)$$

$$\frac{d}{dt} m_{1,\pm 1}^b = -(c_1^b + p_{11}^b \mp i \delta_b) m_{1,\pm 1}^b \mp 3i \Delta_{\text{AC}} m_{2,\pm 1}^b + \frac{\sqrt{2}}{2} i \Omega_{\text{rf}} m_{1,0}^b, \quad (9b)$$

$$\frac{d}{dt} m_{2,0}^b = -(c_2^b + p_{20}^b) m_{2,0}^b + p_{00}^b m_{0,0}^b + \sqrt{\frac{3}{2}} i \Omega_{\text{rf}} (m_{2,1}^b + m_{2,-1}^b) + c_2^{\text{se}} m_{2,0}^a, \quad (9c)$$

$$\frac{d}{dt} m_{2,\pm 1}^b = -(c_2^b + p_{21}^b \mp i \delta_b) m_{2,\pm 1}^b \mp 3i \Delta_{\text{AC}} m_{1,\pm 1}^b + \frac{\sqrt{6}}{2} i \Omega_{\text{rf}} m_{2,0}^b + i \Omega_{\text{rf}} m_{2,\pm 2}^b, \quad (9d)$$

$$\frac{d}{dt} m_{2,\pm 2}^b = -(c_2^b + p_{22}^b \mp 2i \delta_b) m_{2,\pm 2}^b + i \Omega_{\text{rf}} m_{2,\pm 1}^b. \quad (9e)$$

Here Eqs. (9a) and (9b) are the evolutions of rank $k = 1$ moments related to atomic orientation, and Eqs. (9c)–(9e) are the evolutions of rank $k = 2$ moments related to atomic align-

ment. The coefficients $c_k (k = 1, 2)$ represent the relaxation rates caused by the SEC, which involving two effects: (1) the coefficients $c_k^b (k = 1, 2)$ contribute to the longitudinal relax-

ation rates of atomic orientation and alignment and denote the coherence between different Zeeman sublevels of the same manifold; (2) the coefficients c_k^{se} ($k = 1, 2$) allow longitudinal moments $m_{k,0}^b$ for $F_b = 3$ manifold coupled to that of $m_{k,0}^a$ for $F_a = 4$ manifold, leading to a transfer of the population, orientation, and alignment between the two ground states.

Note that Eq. (9) is obtained when we assume the rf frequency ω_{rf} is much larger than the SEC relaxation coefficient c_k^{se} , i.e., $\omega_{\text{rf}} \gg c_k^{\text{se}}$. In that case we show that the SEC process c_k^{se} ($k = 1, 2$) only causes the coupling between longitudinal moments $m_{k,0}^b$ and that of $m_{k,0}^a$ shown in Eqs. (9a) and (9c). In fact, it can be found in Eq. (B1) in Appendix B that the transverse moments $m_{k,q \neq 0}^b$ and transverse moments $m_{k,q \neq 0}^a$ are also coupled by SEC. However, due to the $F_a = 4$ and $F_b = 3$ levels present opposite Larmor precession directions, the coupling between the transverse moments of $m_{k,q \neq 0}^b$ and $m_{k,q \neq 0}^a$ behaves as a fast rf-oscillating term: $c_k^{\text{se}} e^{-2q i \omega_{\text{rf}} t}$ [shown in Eqs. (B1b), (B1d), and (B1e)]. In our system, the value of the rf-frequency ω_{rf} is tuned to (22.0–22.8) kHz, which is much larger than $c_k^{\text{se}} \approx 10$ Hz, then the fast rf-oscillating term can be ignored under the long-time approximation, then Eq. (B1) can be simplified to Eq. (9).

In our calculations, the corresponding coefficients are given by $c_1^b = \frac{37}{64} \Gamma_{\text{se}}$, $c_2^b = \frac{39}{64} \Gamma_{\text{se}}$, $c_1^{\text{se}} = \frac{3\sqrt{105}}{64} \Gamma_{\text{se}}$, $c_2^{\text{se}} = \frac{5\sqrt{33}}{64} \Gamma_{\text{se}}$, where Γ_{se} is the SEC relaxation rate. In addition, the coefficients p_{kq}^b represent the laser-induced equivalent relaxation rate induced by the combined action of the optical

pumping and spontaneous emission, with detailed expressions given in Appendix C. We show that the laser-induced relaxation rates p_{kq}^b not only depend on the Rabi frequency of light Ω_L and the total spontaneous emission rate Γ but also on the detuning $\Delta_{F'}$ ($F' = 2, 3, 4$).

In Eqs. (9b) and (9d) it is the tensor light shift Δ_{AC} that couples atomic vector moments $m_{1,\pm 1}^b$ and second-rank moments $m_{2,\pm 1}^b$. When satisfying $\Delta_{\text{AC}} = 0$, i.e., the pumping light is near resonant to the atomic $F_b = 3 \rightarrow F'$ transition, the evolution of atomic vector moments $m_{1,q}^b$ ($q = -1, 0, 1$) and that of second-rank moments $m_{2,q}^b$ ($q = -2, \dots, 2$) are independent. In this case, the linear polarized light pumps the majority of atoms into an aligned state in the $F_b = 3$ manifold with the values of the orientation components being zero, i.e., $m_{1,q}^b$ ($q = -1, 0, 1$) = 0. However, when $\Delta_{\text{AC}} \neq 0$, the tensor light shift induces the coupling between atomic alignment components $m_{2,\pm 1}^b$ and orientation components $m_{1,\pm 1}^b$, resulting in atomic spin polarization converted from aligned state to oriented state in the $F_b = 3$ manifold. Consequently, values of the orientation components are obtained, and the alignment-to-orientation conversion effect achieved.

The $F_a = 4$ state is not directly coupled to the pumping light (the 9193 GHz detuning of the light reduces the optical excitation). Since the SEC relaxation process c_k^{se} ($k = 1, 2$) cause coupling between the longitudinal moments $m_{k,0}^a$ and that of $m_{k,0}^b$, the evolution equations of atomic multipole moments $m_{k,q}^a$ ($k = 0, 1, 2; q = -k \dots k$) of $F_a = 4$ manifold also need to be considered and can be given by

$$\frac{d}{dt} m_{1,0}^a = -c_1^a m_{1,0}^a - \frac{\sqrt{2}}{2} i \Omega_{\text{rf}} (m_{1,1}^a + m_{1,-1}^a) + (c_1^{\text{se}} + p_{10}^a) m_{1,0}^b, \quad (10a)$$

$$\frac{d}{dt} m_{1,\pm 1}^a = -(c_1^a \pm i \delta_a) m_{1,\pm 1}^a - \frac{\sqrt{2}}{2} i \Omega_{\text{rf}} m_{1,0}^a + p_{11}^a m_{1,\pm 1}^b, \quad (10b)$$

$$\frac{d}{dt} m_{2,0}^a = -c_2^a m_{2,0}^a - \sqrt{\frac{3}{2}} i \Omega_{\text{rf}} (m_{2,1}^a + m_{2,-1}^a) + (c_2^{\text{se}} + p_{20}^a) m_{2,0}^b + p_{00}^a m_{0,0}^b, \quad (10c)$$

$$\frac{d}{dt} m_{2,\pm 1}^a = -(c_2^a \pm i \delta_a) m_{2,\pm 1}^a - \frac{\sqrt{6}}{2} i \Omega_{\text{rf}} m_{2,0}^a - i \Omega_{\text{rf}} m_{2,\pm 2}^a + p_{21}^a m_{2,\pm 1}^b, \quad (10d)$$

$$\frac{d}{dt} m_{2,\pm 2}^a = -(c_2^a \pm 2i \delta_a) m_{2,\pm 2}^a - i \Omega_{\text{rf}} m_{2,\pm 1}^a + p_{22}^a m_{2,\pm 2}^b. \quad (10e)$$

Similar descriptions of the SEC relaxation rates c_k ($k = 1, 2$) and the laser-induced equivalent relaxation rates p_{kq}^a have been given in Eq. (9). For the $F_a = 4$ state, we have $c_1^a = \frac{29}{64} \Gamma_{\text{se}}$, $c_2^a = \frac{31}{64} \Gamma_{\text{se}}$. The expressions of the laser-induced relaxation rates p_{kq}^a are also given in Appendixes A and C. Compared to Eq. (9), the coupling between longitudinal moments $m_{k,0}^a$ and that of $m_{k,0}^b$ relies on the combined effect of the SEC and the laser-induced equivalent relaxation rates. As a consequence of these two factors, part of the atomic population will be transferred from the sublevels of the $F_b = 3$ to that of the $F_a = 4$ state, thereby generating atomic alignment and orientation in the $F_a = 4$ manifold. In order to further illustrate the mechanisms responsible for the AOC effects occurring in two ground states, the numerical analysis of the steady-state

solutions of these multipole moments $\{m_{k,q}^a, m_{k,q}^b\}$ ($k = 0, 1, 2; q = -k \dots k$) will be given in the next section.

III. ANALYTIC EXPRESSION OF ATOMIC POLARIZATION

Now we will investigate the expression of atomic polarization P_i ($i = 1, 2, 3, 4$) described by atomic multipole moments. In Sec. II B the expressions of the change of the light-field parameters in terms of atomic polarization \mathbf{P} have been shown in Eq. (4). By calculating the expectation value of the optical polarization of the medium $\mathbf{P} = n \text{Tr } \rho \mathbf{d}$ (where n is the atomic density) and then transferring the density matrix

elements to atomic multipole moments, the atomic polarization \mathbf{P} can be expressed as

$$\begin{aligned} \mathbf{P} = n \operatorname{Re} \{ & \langle J = 1/2 \| d \| J' = 3/2 \rangle e^{-i\omega t} \\ & \times \left[A_0^b \bar{m}_{0,0}^b - \frac{A_2^b}{\sqrt{3}} \bar{m}_{2,0}^b + \frac{A_2^b}{\sqrt{2}} (\bar{m}_{2,2}^b + \bar{m}_{2,-2}^b) \right] \hat{\mathbf{x}} \\ & + i \left[A_1^b \bar{m}_{1,0}^b + \frac{A_2^b}{\sqrt{2}} (\bar{m}_{2,2}^b - \bar{m}_{2,-2}^b) \right] \hat{\mathbf{y}} \}. \end{aligned} \quad (11)$$

To avoid confusion, we denote the atomic multipole moments as $\bar{m}_{k,q}$ when referring to the laboratory-frame xyz . In Eq. (11), due to the light propagating along the z axis, the atomic polarization component in that direction must be zero. We observe that the polarization along x axis is determined by the second-rank moments $\bar{m}_{2,q}^b (q = 0, \pm 2)$, while one along y axis relies on the longitudinal vector moment $\bar{m}_{1,0}^b$ and the transversal second-rank moments $\bar{m}_{2,\pm 2}^b$. Coefficients $A_k^b (k = 0, 1, 2)$ are the absorption coefficients corresponding to atomic k -rank moments of the $F_b = 3$ level, and given by

$$A_0^b = \frac{i\Omega_L}{\sqrt{7}} \left[-\frac{20}{3(\Gamma + 2i\Delta_2)} - \frac{7}{(\Gamma + 2i\Delta_3)} - \frac{5}{(\Gamma + 2i\Delta_4)} \right], \quad (12a)$$

$$A_1^b = \frac{i\Omega_L}{\sqrt{7}} \left[\frac{20}{3(\Gamma + 2i\Delta_2)} + \frac{7}{4(\Gamma + 2i\Delta_3)} - \frac{15}{4(\Gamma + 2i\Delta_4)} \right], \quad (12b)$$

$$A_2^b = \frac{i\Omega_L}{\sqrt{7}} \left[\frac{4}{(\Gamma + 2i\Delta_2)} - \frac{21}{4(\Gamma + 2i\Delta_3)} + \frac{5}{4(\Gamma + 2i\Delta_4)} \right]. \quad (12c)$$

We see the absorption coefficients $A_k^b (k = 0, 1, 2)$ are dominated by the Rabi frequency Ω_L of the light field, the total spontaneous emission rate Γ , and the detuning $\Delta_{F'} (F' = 2, 3, 4)$.

Comparing Eqs. (11) and (2), the polarization components $P_{1,2,3,4}$ can be given by

$$P_1 = \langle J = 1/2 \| d \| J' = 3/2 \rangle n \operatorname{Re} \left[A_0^b \bar{m}_{0,0}^b - \frac{A_2^b}{\sqrt{3}} \bar{m}_{2,0}^b + \frac{A_2^b}{\sqrt{2}} (\bar{m}_{2,2}^b + \bar{m}_{2,-2}^b) \right], \quad (13a)$$

$$P_2 = -\langle J = 1/2 \| d \| J' = 3/2 \rangle n \operatorname{Im} \left[A_0^b \bar{m}_{0,0}^b - \frac{A_2^b}{\sqrt{3}} \bar{m}_{2,0}^b + \frac{A_2^b}{\sqrt{2}} (\bar{m}_{2,2}^b + \bar{m}_{2,-2}^b) \right], \quad (13b)$$

$$P_3 = -\langle J = 1/2 \| d \| J' = 3/2 \rangle n \operatorname{Im} \left[A_1^b \bar{m}_{1,0}^b + \frac{A_2^b}{\sqrt{2}} (\bar{m}_{2,2}^b - \bar{m}_{2,-2}^b) \right], \quad (13c)$$

$$P_4 = -\langle J = 1/2 \| d \| J' = 3/2 \rangle n \operatorname{Re} \left[A_1^b \bar{m}_{1,0}^b + \frac{A_2^b}{\sqrt{2}} (\bar{m}_{2,2}^b - \bar{m}_{2,-2}^b) \right]. \quad (13d)$$

In laboratory-frame xyz , we see the polarization parameters $P_{1,2}$ related to the x direction polarization are dominated by the second-rank moments $\bar{m}_{2,q}^b (q = 0, \pm 2)$. Meanwhile, the $P_{3,4}$ related to the y direction polarization are determined by vector moments $\bar{m}_{1,0}^b$ and second-rank moments $\bar{m}_{2,q}^b (q = \pm 2)$.

Note that our calculations shown in Sec. IID are carried out in the rotation frame $x'y'z'$, which allows us to rotate the polarization parameters from the laboratory-frame xyz to the rotating frame $x'y'z'$ by applying the Wigner D function

$$\bar{m}_{k,q} = \sum_{q'} \tilde{m}_{k,q'} D_{q'q}^{(k)}(0, \frac{\pi}{2}, -\pi)^*. \quad (14)$$

Here $D_{q'q}^{(k)}$ represents the Wigner D function [33]. Atomic multipole moments $\bar{m}_{k,q}$ and $\tilde{m}_{k,q'}$ are, respectively, defined in the laboratory-frame xyz and in the rotation frame $x'y'z'$. Inserting Eq. (14) into Eq. (13), the expressions of the parameters $P_{1,2,3,4}$ in rotating frame can be written as

$$P_1 = \langle J = 1/2 \| d \| J' = 3/2 \rangle n \operatorname{Re} \left[A_0^b \tilde{m}_{0,0}^b + \frac{2A_2^b}{\sqrt{3}} \tilde{m}_{2,0}^b \right], \quad (15a)$$

$$P_2 = -\langle J = 1/2 \| d \| J' = 3/2 \rangle n \operatorname{Im} \left[A_0^b \tilde{m}_{0,0}^b + \frac{2A_2^b}{\sqrt{3}} \tilde{m}_{2,0}^b \right], \quad (15b)$$

$$P_3 = -\langle J = 1/2 \| d \| J' = 3/2 \rangle n \operatorname{Im} \left[\frac{A_1^b}{\sqrt{2}} (\tilde{m}_{1,1}^b - \tilde{m}_{1,-1}^b) - \frac{A_2^b}{\sqrt{2}} (\tilde{m}_{2,1}^b + \tilde{m}_{2,-1}^b) \right], \quad (15c)$$

$$P_4 = -\langle J = 1/2 \| d \| J' = 3/2 \rangle n \operatorname{Re} \left[\frac{A_1^b}{\sqrt{2}} (\tilde{m}_{1,1}^b - \tilde{m}_{1,-1}^b) - \frac{A_2^b}{\sqrt{2}} (\tilde{m}_{2,1}^b + \tilde{m}_{2,-1}^b) \right]. \quad (15d)$$

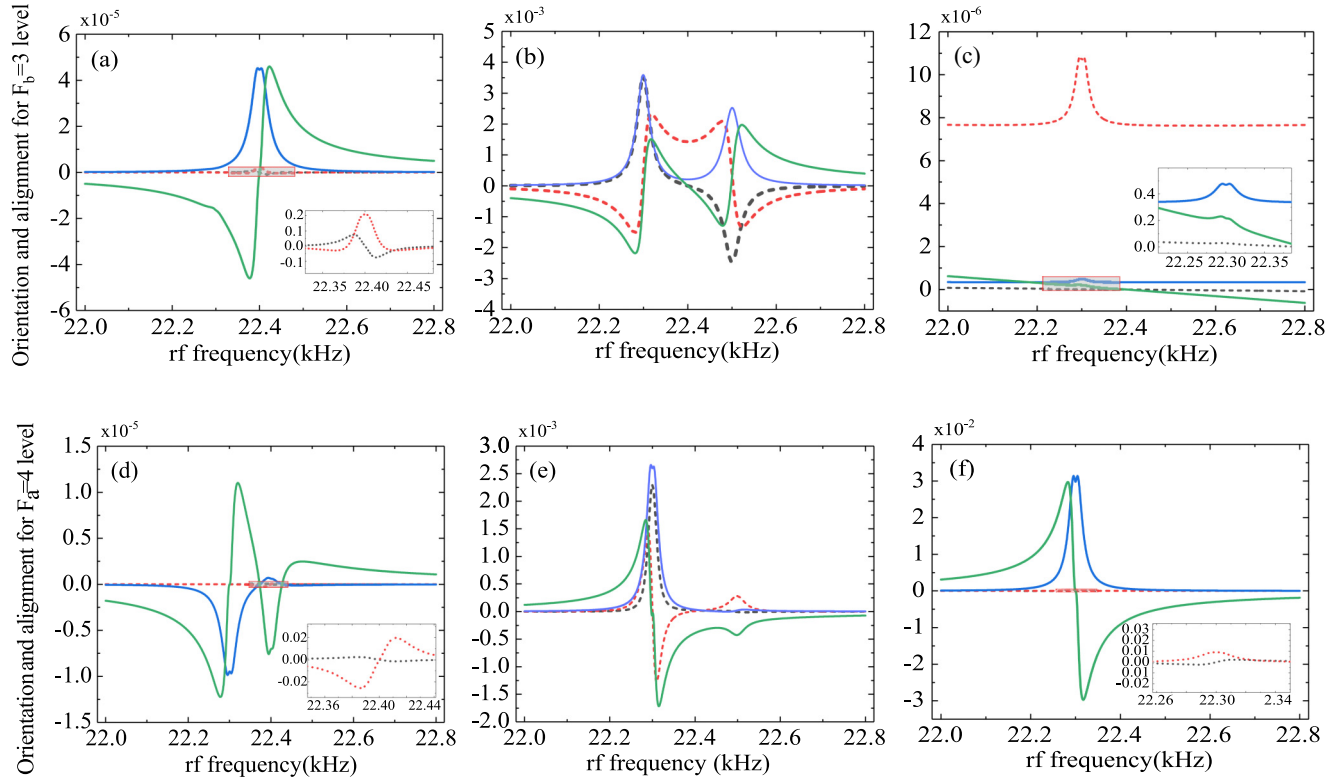


FIG. 2. The steady-state values of atomic orientation and alignment components for the two ground states as a function of rf frequency for different light powers. Blue solid lines: The imaginary part of $m_{2,-1}^b$ (a)–(c) or $m_{2,-1}^a$ (d) and (e). Green solid lines: The real part of $m_{2,-1}^b$ (a)–(c) or $m_{2,-1}^a$ (d) and (e). Black dotted line: The imaginary part of $m_{1,-1}^b$ (a)–(c) or $m_{1,-1}^a$ (d) and (e). Red dotted line: The real part of $m_{1,-1}^b$ (a)–(c) or $m_{1,-1}^a$ (d) and (e). (a) and (d) $\Omega_L = 1 \times 10^4$ Hz, (b) and (e) $\Omega_L = 1.43 \times 10^5$ Hz, (c) and (f) $\Omega_L = 1 \times 10^6$ Hz. Here natural linewidth $\Gamma = 6$ MHz, SEC relaxation rate $\Gamma_{se} = 3 \times 10^{-6}\Gamma$, Rabi frequency of rf field $\Omega_{rf} = 1 \times 10^{-6}\Gamma$, light detuning $\Delta_2 = -100$ MHz.

Equation (15) shows that the polarization parameters $P_{1,2}$ are dominated by the longitudinal moment $\tilde{m}_{0,0}^b$ and the second-rank moment $\tilde{m}_{2,0}^b$, and the parameters $P_{3,4}$ rely on atomic vector moments $\tilde{m}_{1,\pm 1}^b$ and second-rank tensor moments $\tilde{m}_{2,\pm 1}^b$. The time-dependent polarization moments $\tilde{m}_{k,q}$ in Eq. (15) satisfies $\tilde{m}_{k,q}^b = m_{k,q}^b e^{qi\omega_{rf}t}$, where $m_{k,q}^b$ denotes atomic multipole moments after applying the rotating-wave approximation in terms of the rf field, i.e., the steady-state solutions of the Eqs. (9) and (10).

In Fig. 2 we plot the steady-state values of orientation and alignment components of the two ground states as a function of rf frequency for different light power regimes. When the Rabi frequency of the pump light is weak, as shown in Figs. 2(a) and 2(d), the steady-state values of the components of atomic alignment $m_{2,\pm 1}^b$ and $m_{2,\pm 1}^a$ are much greater than the components of orientation $m_{1,\pm 1}^b$ and $m_{1,\pm 1}^a$. For the $F_b = 3$ state, the coupling between atomic alignment and orientation is weak due to the small tensor light shift, and this state can be regarded as the aligned state. The imaginary and real part of $m_{2,\pm 1}^b$ consists of large symmetric and antisymmetric features when the rf frequency is tuned to the Larmor frequency of the $F_b = 3$ state (22.4 kHz), with a much smaller structure due to the off-resonant excitation into the $F_a = 4$ state (22.3 kHz).

When we choose the Rabi frequency of the pump light $\Omega_L = 14.3 \times 10^4$ Hz that satisfies $\delta_a = \delta_b + 3\Delta_{AC}$, the coupling between the ground states $F_b = 3$ and $F_a = 4$ reaches the maximum. Meanwhile, the resonance responses of the

moments $\{m_{k,\pm 1}^a, m_{k,\pm 1}^b\}$ ($k = 1, 2$) appear in the regimes where the rf frequency is tuned to be approximately 22.3 and 22.5 kHz, as shown in Figs. 2(b) and 2(e). This particular point can be understood in the following way. As shown in Eq. (9), the matrix form of the evolution equations that only consider the tensor light shift Δ_{AC} can be expressed as

$$\begin{pmatrix} \dot{m}_{1,1}^b \\ \dot{m}_{2,1}^b \end{pmatrix} = \begin{pmatrix} \delta_b & -3\Delta_{AC} \\ -3\Delta_{AC} & \delta_b \end{pmatrix} \begin{pmatrix} m_{1,1}^b \\ m_{2,1}^b \end{pmatrix}. \quad (16)$$

The eigenvalues of Eq. (16) are $V_E^{(\pm)} = \delta_b \pm 3\Delta_{AC}$, and the corresponding eigenstates are $S_E^{(\pm)} = m_{1,\pm 1}^b \pm m_{2,\pm 1}^b$. As shown in Fig. 3, when the rf frequency ω_{rf} is tuned to $\delta_b \pm \Delta_{AC}$, $\delta_b \pm 3\Delta_{AC}$, or $\delta_b \pm 5\Delta_{AC}$, the single-photon resonance occurs between different adjacent Zeeman sublevels. We observe that the equivalent transitions of atomic multipole moments related to the eigenvalues $V_E^{(\pm)}$ can be interpreted as the results of equal probability superposition of each single photon transitions, which can be written as $V_E^{(\pm)} = [(\delta_b \pm \Delta_{AC}) + (\delta_b \pm 3\Delta_{AC}) + (\delta_b \pm 5\Delta_{AC})]/3$. In this case, the steady-state values of atomic alignment $m_{2,\pm 1}^b$ and orientation $m_{1,\pm 1}^b$ can be observed simultaneously. Meanwhile, the values of $m_{k,\pm 1}^b$ are in the same order of magnitude as that of $m_{k,\pm 1}^a$, which reveals that the total atoms are approximately evenly distributed in the two ground states. Due to the significant coupling between moments $m_{2,\pm 1}^b$ and $m_{1,\pm 1}^b$ induced by the tensor AC-Stark effect, we observe that the degree of spin orientation is comparable to that of alignment in the $F_b = 3$

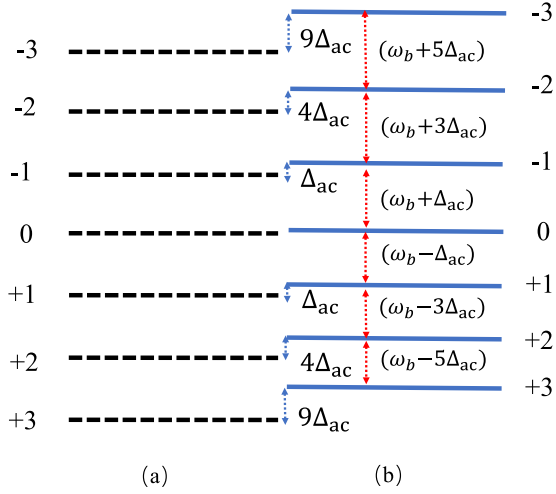


FIG. 3. Energy structure of the $F_b = 3$ manifold. (a) Linear Zeeman effect. The black-dotted lines denote the Zeeman sublevels splitted by linear Zeeman effect. (b) Considering tensor Stark effect. The blue-solid lines are the Zeeman sublevels considering the tensor light shift Δ_{AC} . The red arrows represent the single-photon resonance transitions.

manifold. Eventually, alignment-to-orientation conversion is achieved. For the $F_a = 4$ state, spin orientation generates indirectly due to the combined action of a direct orientation of the $F_b = 3$ states and SEC. The steady-state value of orientation $m_{1,\pm 1}^a$ is also comparable to that of alignment $m_{2,\pm 1}^a$, indicating that AOC also occurs in the $F_a = 4$ manifold.

Figures 2(c) and 2(f) show the steady-state values of the orientation and alignment components as a function of rf frequency when the light power is relatively strong. In this case, strong optical transfer disturbs the population balance between the two hyperfine manifolds such that occupation of the $F_a = 4$ manifold exceeds that of the $F_b = 3$. This results in a reduction of the amplitude of the rf resonance observed in the $F_b = 3$ state as its population is removed. In addition, the tensor AC-Stark effect leads to a drastic transfer of atomic polarization from the alignment to orientation, as a result, the steady-state values of atomic orientation moments $m_{1,\pm 1}^b$ are considerably greater than those of the alignment moments $m_{2,\pm 1}^b$. As shown in Fig. 2(c), the real part of the orientation moments $m_{1,\pm 1}^b$ has the symmetric feature when the rf frequency is tuned to the vicinity of 22.3 kHz. For the $F_a = 4$ state, the majority of atoms are clustered in this state and the aligned polarization rate created by the optical pumping is greater than the depolarization rate caused by the rf field and SEC processes. That results in the values of $m_{2,\pm 1}^a$ are much greater than $m_{1,\pm 1}^a$. As shown in Fig. 2(f), the imaginary and real parts of $m_{2,\pm 1}^a$ consist of large symmetric and antisymmetric features when the rf frequency is tuned to the Larmor frequency of the $F_a = 4$ state (22.3 kHz).

IV. MAGNETO-OPTICAL ROTATION SIGNALS

Now we are going to investigate the magneto-optical rotation rf signals in our system. As described in Eq. (4), the optical-rotation α is determined by the polarization component P_4 shown in Eq. (15d). Therefore, the in-phase and

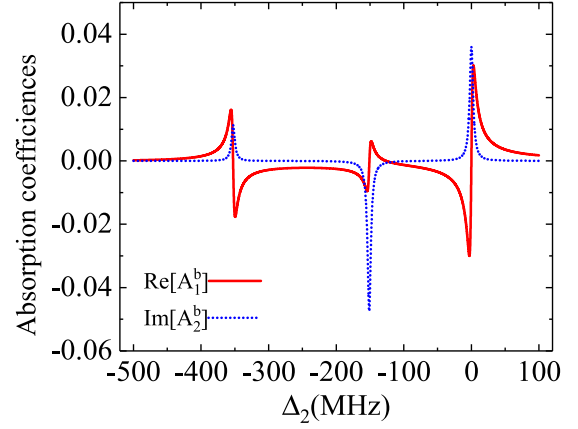


FIG. 4. Atomic absorption coefficients as a function of the optical detuning Δ_2 . Red line: The real part of A_1^b , blue line: the imaginary part of A_2^b .

quadrature (out-of-phase) of the signals per unit length dz of the medium are

$$\frac{d\alpha^{\text{in}}}{dz} = \frac{n\Gamma\lambda^2}{4\pi\Omega_L} \left\{ -\text{Re}[A_1^b](m_{1,1}^b - m_{1,-1}^b) + i\text{Im}[A_2^b](m_{2,1}^b + m_{2,-1}^b) \right\}, \quad (17)$$

$$\frac{d\alpha^{\text{out}}}{dz} = \frac{n\Gamma\lambda^2}{4\pi\Omega_L} \left\{ -\text{Im}[A_2^b](m_{2,1}^b - m_{2,-1}^b) - i\text{Re}[A_1^b](m_{1,1}^b + m_{1,-1}^b) \right\}. \quad (18)$$

Here λ is the transition wavelength, and n is the atomic density. We show that the optical-rotation signals rely on a product of two factors: atomic alignment $m_{2,\pm 1}^b$ and orientation $m_{1,\pm 1}^b$ of the $F_b = 3$ manifold, and the corresponding absorption coefficients A_k^b ($k = 1, 2$).

Figure 4 shows the dependence of atomic absorption coefficients A_k^b ($k = 1, 2$) on the optical detuning Δ_2 . The red line shows the real part of the one-rank absorption coefficient A_1^b and presents antisymmetric features, and the blue line represent the imaginary part of the second-rank absorption coefficient A_2^b and presents symmetric features. The resonance response occurs when the laser frequency is in the vicinity of the $F_b = 3 \rightarrow F' = 2, 3, 4$ transition.

Figures 5(a)–5(c) show the in-phase and quadrature optical rotation signals as a function of rf frequency for three distinct light powers at the detuning $\Delta_2 = -100$ MHz. In Fig. 5(a), when $\Omega_L = 1 \times 10^4$ Hz, the optical rotation signals are mainly determined by atomic alignment with minor orientation contribution. This is because the value of atomic alignment $m_{2,\pm 1}^b$ is much larger than that of the orientation $m_{1,\pm 1}^b$. This results in the in-phase and quadrature components presenting large antisymmetric and symmetric features when the rf frequency is equal to the Larmor frequency of the $F_b = 3$ state, with a considerably smaller structure when the rf frequency is equal to the Larmor frequency of the $F_a = 4$ state. However, as the Rabi frequency of the optical pump increases to $\Omega_L = 1.43 \times 10^5$ Hz, the degrees of atomic alignment and orientation are comparable, while the real part of the coefficient A_1^b is larger than the imaginary part of A_2^b .

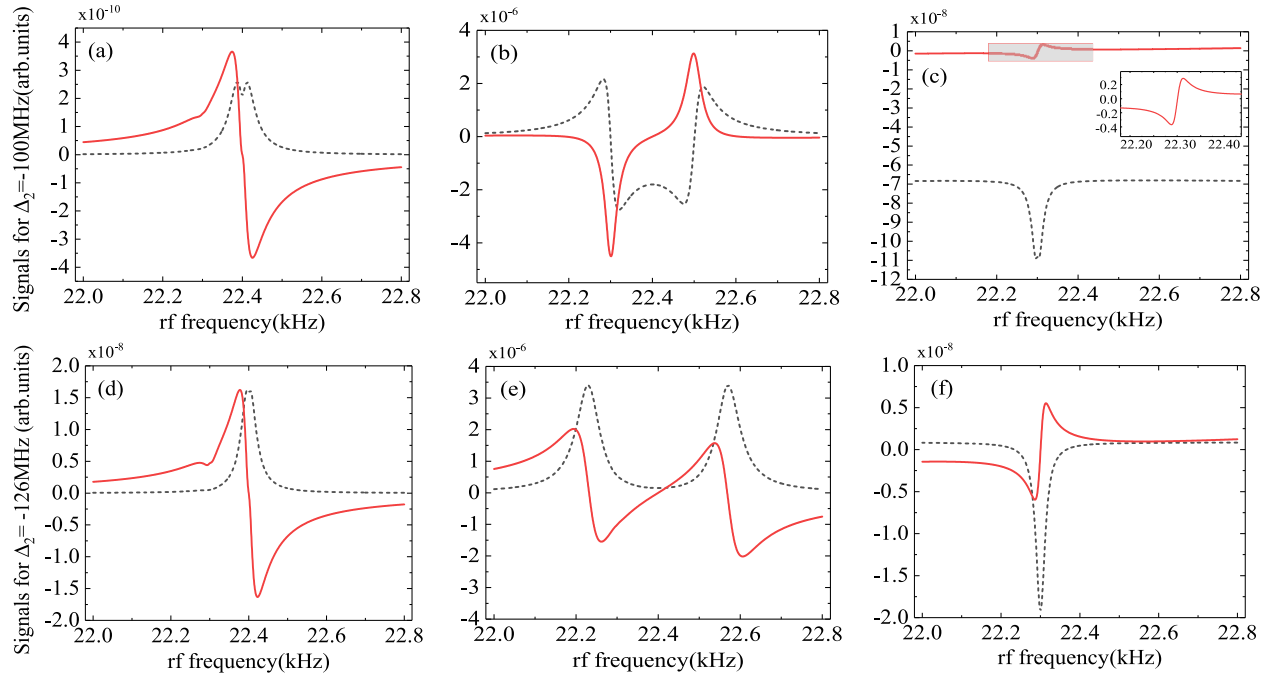


FIG. 5. The in-phase (red solid lines) and quadrature (black dotted lines) components of magneto-optical rotation signals as a function of rf frequency for different light powers. (a)–(c) $\Delta_2 = -100$ MHz, (d)–(f) $\Delta_2 = -126$ MHz. Reduced Rabi frequency of the pumping light: left $\Omega_L = 1 \times 10^4$ Hz, middle $\Omega_L = 1.43 \times 10^5$ Hz, right $\Omega_L = 1 \times 10^6$ Hz. Natural linewidth $\Gamma = 6$ MHz, SEC relaxation rate $\Gamma_{se} = 3 \times 10^{-6}\Gamma$, Rabi frequency of rf field $\Omega_{rf} = 1 \times 10^{-6}\Gamma$.

This results in that the optical-rotation signals mainly rely on the orientation $m_{1,\pm 1}^b$ contribution and the resonance response appears when the rf frequency is tuned to 22.3 and 22.5 kHz, which reflects the AOC effect occurring in the $F_b = 3$ manifold. As the Rabi frequency of the optical pump increases to $\Omega_L = 1 \times 10^7$ Hz, the value of atomic orientation $m_{1,\pm 1}^b$ becomes considerably greater than that of the alignment $m_{2,\pm 1}^b$ and dominates the optical-rotation signals. Consequently, the in-phase and quadrature components present antisymmetric and symmetric features with the resonance response appears in the vicinity of 22.3 kHz, as shown in Fig. 5(c).

Note that the light detuning Δ_2 not only determines the laser-induced equivalent relaxation rates but also affects the values of the absorption coefficients, resulting in significantly affecting the magneto-optical rotation signals. Figures 5(d) and 5(e) show the in-phase and quadrature optical rotation signals as a function of rf frequency for three distinct light powers at $\Delta_2 = -126$ MHz. In that case, the real part of the one-rank absorption coefficient A_1^b is equal to the imaginary part of the second-rank A_2^b . Eventually, the optical rotation signals are determined by the atomic orientation and alignment with equal weights. The evolution processes of atomic multipole moments are similar to those depicted in Figs. 5(a)–5(c), however, the light detuning can significantly impact the line shape of the optical rotation signals.

V. CONCLUSION

In conclusion, we present a theoretical study of the MOR effect in cesium atoms in the Voigt geometry, in which the simplified description of AOC is presented using atomic multipole moments instead of the standard density-matrix theory.

We have shown that due to the tensor AC-Stark effect, one can achieve AOC effect in the ground state $F_b = 3$ manifold. While the orientation in the $F_a = 4$ manifold builds up by the indirect pumping combined with the SEC process. In addition, the analytical expression of atomic polarization parameter \mathbf{P} described by atomic multipole moments is obtained. Moreover, the contributions of the AOC effect to the optical-rotation signals are discussed in different light power regimes. Although we only applied the theoretical study to the D_2 line of Cs atoms, the results for other alkali-metal atoms [35] or even other structures such as nitrogen-vacancy centers [13] are expected to be similar. Our results may be helpful for guiding MOR experiments by refining and optimizing the parameters [31].

ACKNOWLEDGMENT

This work is supported by the National Natural Science Foundation of China (Grant No. 12174139).

APPENDIX A: HAMILTONIAN IN THE SYSTEM

In our system, the calculations are carried out in the rotation frame $x'y'z'$ shown in Fig. 1(c). The total Hamiltonian H_{total} is given by

$$H_{\text{total}} = H_0 + H'_L + \tilde{H}_B, \quad (\text{A1})$$

where H_0 is the unperturbed part of the Hamiltonian, describing the energy structure of the ground (unprimed quantities)

and the excited (primed quantities) states

$$H_0 = \sum_{FM_F} \omega_{FM_F} |FM_F\rangle \langle FM_F| + \sum_{F'M'_F} \omega_{F'M'_F} |F'M'_F\rangle \langle F'M'_F|, \quad (\text{A2})$$

with ω_{FM_F} and $\omega_{F'M'_F}$ being the energy of the ground state $|FM_F\rangle$ and excited state $|F'M'_F\rangle$, respectively, where F and F' denotes the total atomic angular momentum quantum numbers of the ground and excited levels and M_F and M'_F are the corresponding magnetic quantum numbers of the levels. In our system, the basis of states $\{|FM_F\rangle, |F'M'_F\rangle\}$ is

$$\begin{aligned} |FM_F\rangle &= |4, +4\rangle, \dots, |4, -4\rangle, |3, +3\rangle, \dots, |3, -3\rangle, \quad (\text{A3}) \\ |F'M'_F\rangle &= |5', +5'\rangle, \dots, |5', -5'\rangle, |4', +4'\rangle, \dots, |4', -4'\rangle, \\ &|3', +3'\rangle, \dots, |3', -3'\rangle, |2', +2'\rangle, \dots, |2', -2'\rangle. \end{aligned} \quad (\text{A4})$$

The detailed expressions of the light-atom interaction Hamiltonian H'_L and the magnetic field interaction Hamiltonian \tilde{H}_B are given in the next subsection.

1. Light-atom interaction and spontaneous emission

As shown in Fig. 1, the atomic ensemble is optically pumped by a linearly polarized laser beam. Choosing the light polarization direction (z') as the quantization axis in the rotation frame $x'y'z'$, the light-atom interaction Hamiltonian is given by $H'_L = -\mathbf{E} \cdot \mathbf{d} = -E_0 \cos(\omega_L t) d_{z'}$, where E_0 is the amplitude of the light field, and ω_L is the laser frequency. By applying the rotating-wave approximation and transition rules, in our system, the Hamiltonian H'_L can be given by an explicit form

$$H'_L = \frac{1}{2} \Sigma' + \Omega_L^* \Sigma_0 + \Omega_L \Sigma_0^\dagger. \quad (\text{A5})$$

Here $\Omega_L = -E_0 \langle J || \mathbf{d} || J' \rangle$ denotes the reduced Rabi frequency of the pumping light, where $\langle J || \mathbf{d} || J' \rangle$ is the reduced matrix element that depends only on the L , S , and J quantum numbers. The operators Σ' and Σ_0 are defined as

$$\Sigma' = \sum_{F'=2,3,4} \sum_{M'_F} \Delta_{F'} |F'M'_F\rangle \langle F'M'_F|, \quad (\text{A6})$$

$$\Sigma_0 = \sum_{F'=2,3,4} \sum_{F=3} \Sigma_0^{FF'}. \quad (\text{A7})$$

In Eq. (A6), $\Delta_{F'} = \omega_{F_b F'} - \omega_L$ is the detuning of the atomic transition $F_b = 3 \rightarrow F'$ frequency and the laser field frequency. Note that we assume the $F_b = 3$ state is directly coupled to the pump light, while the $F_a = 4$ state is not coupled to light (the 9193 MHz detuning of the light reduces the optical excitation). In Eq. (A7), the operator $\Sigma_0^{FF'}$ denotes the q -transition operator that couples two hyperfine energy levels F and F' , where the spherical component $q = 0$ corresponds to $M_F \rightarrow M'_F = M_F$, $q = 1$ corresponds to $M_F \rightarrow M'_F = M_F + 1$, and $q = -1$ corresponds to $M_F \rightarrow M'_F = M_F - 1$. The detailed expression is given by

$$\Sigma_q^{FF'} = \sum_{M_F} V_{FM_F}^{F'M'_F+q} |F'M'_F+q\rangle \langle FM_F|. \quad (\text{A8})$$

According to Wigner-Eckart theorem [3], the transition coefficient $V_{FM_F}^{F'M'_F+q}$ is given by

$$V_{FM_F}^{F'M'_F+q} = (-1)^{M_F+J+I} \sqrt{(2F+1)(2F'+1)(2J+1)} \times \begin{pmatrix} F' & 1 & F \\ M_F+q & q & -M_F \end{pmatrix} \begin{Bmatrix} J & J' & 1 \\ F' & F & I \end{Bmatrix}. \quad (\text{A9})$$

Here the symbols $\begin{pmatrix} \dots \end{pmatrix}$ and $\begin{Bmatrix} \dots \end{Bmatrix}$ are the Wigner 3-j symbol and Wigner 6-j symbol, respectively. I is the nuclear spin, and J and J' are the electron angular momentum of the ground and excited state, respectively.

In addition, the spontaneous emission relaxation process $\mathcal{L}_{sp}\rho$ in our system can also be calculated by the transition operator $\Sigma_q^{FF'}$, which contains multiple relaxation channels and takes the form

$$\mathcal{L}_{sp}\rho = \Gamma \sum_{F'=2,3,4,5} \sum_{F=3,4} \sum_{q=0,\pm 1} D[\Sigma_q^{FF'}] \rho, \quad (\text{A10})$$

where Γ is the total spontaneous emission rate from the excited level. The operator

$$D[\Sigma_q^{FF'}] \rho = \Sigma_q^{FF'} \rho \Sigma_q^{FF'\dagger} - \frac{1}{2} \Sigma_q^{FF'\dagger} \Sigma_q^{FF'} \rho - \frac{1}{2} \rho \Sigma_q^{FF'\dagger} \Sigma_q^{FF'} \quad (\text{A11})$$

is the Lindblad superoperator.

Considering that the spontaneous emission relaxation rate is much greater than the pumping rate of the laser, i.e., $\Gamma \gg \Omega_L$, the excited states $F' = 2, 3, 4, 5$ can be adiabatically eliminated. Therefore, in our system, the basis of states $\{|FM_F\rangle, |F'M'_F\rangle\}$ involving both ground states and excited states reduces to the ground-state subspace $\{|FM_F\rangle\} = \{|F_a M_{F_a}\rangle, |F_b M_{F_b}\rangle\}$. Consequently, the combination of the optical-pumping process and the spontaneous emission relaxation process is equivalent to two effects in the ground-state subspace: the AC-Stark effect and the laser-induced equivalent relaxation process. The equivalent light-field Hamiltonian \tilde{H}_L corresponding to the AC-Stark effect is given by

$$\tilde{H}_L = \Delta_{AC} (F_z^{(b)})^2. \quad (\text{A12})$$

Here $F^{(b)}$ is the angular momentum operators applied to the ground state $F_b = 3$, Δ_{AC} denotes the tensor AC-Stark shift, and the speltic expression is given by Eq. (6) in Sec. II C. The laser-induced equivalent relaxation $\mathcal{L}_L \tilde{\rho}$ takes the form

$$\mathcal{L}_L \tilde{\rho} = \sum_{F'=2,3,4} \frac{16\Gamma}{\Gamma^2 + 4\Delta_{F'}^2} \sum_{q=0,\pm 1} (D[\tilde{\Sigma}_q^{ab}] \tilde{\rho} + D[\tilde{\Sigma}_q^{bb}] \tilde{\rho}), \quad (\text{A13})$$

where $D[\]$ is the Lindblad superoperator given by Eq. (A11). The equivalent transition operator $\tilde{\Sigma}_q^{bb}$ couples energy levels $|F_b M_{F_b}\rangle$ and $|F_b M_{F_b} + q\rangle$, with $q = 0, \pm 1$ for the spherical components. Similarly, the equivalent transition operator $\tilde{\Sigma}_q^{ab}$ couples energy levels $|F_b M_{F_b}\rangle$ and $|F_a M_{F_b} + q\rangle$. The explicit expression satisfies

$$\tilde{\Sigma}_q^{bb} = \sum_{M_{F_b}} V_{F'_i M_{F_b}}^{F_b M_{F_b}+q} V_{F_b M_{F_b}}^{F'_i M_{F_b}} |F_b M_{F_b} + q\rangle \langle F_b M_{F_b}|, \quad (\text{A14})$$

$$\tilde{\Sigma}_q^{ab} = \sum_{M_{F_b}} V_{F'_i M_{F_b}}^{F_a M_{F_b}+q} V_{F_b M_{F_b}}^{F'_i M_{F_b}} |F_a M_{F_b} + q\rangle \langle F_b M_{F_b}|, \quad (\text{A15})$$

where the transition coefficient $V_{FM_F}^{F'M'_F}$ is defined in Eq. (A9).

2. Magnetic field interaction Hamiltonian

In the rotation frame $x'y'z'$ and in the ground-state subspace $\{|FM_F\rangle\}$, the total magnetic field interaction Hamiltonian consists of two parts: Hamiltonian \tilde{H}_{B_0} for a z' -directed magnetic field \mathbf{B}_0 , and a Hamiltonian $\tilde{H}_{B_{\text{rf}}}$ for a field \mathbf{B}_{rf} applied along x' oscillating at the frequency ω_{rf} ,

$$\tilde{H}_B = \tilde{H}_{B_0} + \tilde{H}_{B_{\text{rf}}}. \quad (\text{A16})$$

Here the \tilde{H}_{B_0} is given by

$$\tilde{H}_{B_0} = -\boldsymbol{\mu} \cdot \mathbf{B}_0 = \omega_a F_z^{(a)} - \omega_b F_z^{(b)}, \quad (\text{A17})$$

where $\omega_a = \mu_B |g_{F_a}| B_0$ and $\omega_b = \mu_B |g_{F_b}| B_0$ are the Larmor frequencies of the two hyperfine ground states $F_a = 4$ and $F_b = 3$, respectively. μ_B is the Bohr magneton, and g_{F_a} and g_{F_b} are the corresponding Landé g factors for the $F_a = 4$ and $F_b = 3$ levels. Note that g_{F_a} and g_{F_b} present opposite directions and different values, and can be explained by the g -factor expression, given by

$$g_F = g_J \frac{F(F+1) - I(I+1) + J(J+1)}{2F(F+1)} + g_I \frac{F(F+1) + I(I+1) - J(J+1)}{2F(F+1)}. \quad (\text{A18})$$

In general, the nuclear factor g_I can be neglected in most experiments since it is much smaller than g_J . However, for the magnetic field \mathbf{B}_0 in our system, the nuclear term can induce a significant correction, which is important for precision measurements.

The rf-magnetic field interaction Hamiltonian is given by $\tilde{H}_{\text{rf}} = -\boldsymbol{\mu} \cdot \mathbf{B}_{\text{rf}} = \Omega_{\text{rf}}(F_{x'}^{(a)} - F_{x'}^{(b)}) \cos \omega_{\text{rf}} t$. Using the rotating-wave approximation, the Hamiltonian \tilde{H}_{rf} can be given by an explicit form

$$\tilde{H}_{\text{rf}} = \Omega_{\text{rf}}(F_+^{(a)} e^{-i\omega_{\text{rf}} t} + F_-^{(a)} e^{i\omega_{\text{rf}} t}) - \Omega_{\text{rf}}(F_+^{(b)} e^{i\omega_{\text{rf}} t} + F_-^{(b)} e^{-i\omega_{\text{rf}} t}). \quad (\text{A19})$$

Due to the rf field is much weaker than the static magnetic field, the Rabi frequency of the rf field corresponding to

$$\dot{m}_{1,0}^b = -(c_1^b + p_{10}^b) m_{1,0}^b + \frac{\sqrt{2}}{2} i \Omega_{\text{rf}} (m_{1,1}^b + m_{1,-1}^b) + c_1^{\text{se}} m_{1,0}^a, \quad (\text{B1a})$$

$$\dot{m}_{1,\pm 1}^b = -(c_1^b + p_{11}^b \mp i\delta_b) m_{1,\pm 1}^b \mp 3i\Delta_{\text{AC}} m_{2,\pm 1}^b + \frac{\sqrt{2}}{2} i \Omega_{\text{rf}} m_{1,0}^b + c_1^{\text{se}} m_{1,\pm 1}^a e^{\mp 2i\omega_{\text{rf}} t}, \quad (\text{B1b})$$

$$\dot{m}_{2,0}^b = -(c_2^b + p_{20}^b) m_{2,0}^b + p_{00}^b m_{0,0}^b + \sqrt{\frac{3}{2}} i \Omega_{\text{rf}} (m_{2,1}^b + m_{2,-1}^b) + c_2^{\text{se}} m_{2,0}^a, \quad (\text{B1c})$$

$$\dot{m}_{2,\pm 1}^b = -(c_2^b + p_{21}^b \mp i\delta_b) m_{2,\pm 1}^b \mp 3i\Delta_{\text{AC}} m_{1,\pm 1}^b + \frac{\sqrt{6}}{2} i \Omega_{\text{rf}} m_{2,0}^b + i \Omega_{\text{rf}} m_{2,\pm 2}^b + c_2^{\text{se}} m_{2,\pm 1}^a e^{\mp 2i\omega_{\text{rf}} t}, \quad (\text{B1d})$$

$$\dot{m}_{2,\pm 2}^b = -(c_2^b + p_{22}^b \mp 2i\delta_b) m_{2,\pm 2}^b + i \Omega_{\text{rf}} m_{2,\pm 1}^b + c_2^{\text{se}} m_{2,\pm 2}^a e^{\mp 4i\omega_{\text{rf}} t}. \quad (\text{B1e})$$

In Eq. (B1) we see that the SEC relaxation process c_k^{se} causes atomic multipole moment $\tilde{m}_{k,q}^b$ coupled to the moment $\tilde{m}_{k,q}^a$,

two hyperfine ground states can be assumed to be the same $\Omega_{\text{rf}} = 1/2 \mu_B |g_F| B_{\text{rf}}$. The components of the angular momentum operator $F(F^{(a)}, F^{(b)})$ obey

$$F_z |F, M_F\rangle = M_F |F, M_F\rangle,$$

$$F_{\pm} |F, M_F\rangle = \sqrt{(F \pm M_F + 1)(F \mp M_F)} |F, M_F \pm 1\rangle. \quad (\text{A20})$$

To calculate slow evolution of the density matrix, we apply the frame rotating at the rf frequency ω_{rf} to the Hamiltonian \tilde{H}_{rf} ,

$$\tilde{H}_{\text{rf}}^{\text{rot}} = U^+ \tilde{H}_{\text{rf}} U - iU^+ \frac{dU}{dt}, \quad (\text{A21})$$

where $U = e^{-i\omega_{\text{rf}}(F_z^{(a)} - F_z^{(b)})t}$ is a diagonal unitary transformation matrix, to remove the fast oscillating component from the density-matrix evolution. Therefore, the total magnetic field interaction Hamiltonian at the frame rotating takes the form

$$\tilde{H}_B^{\text{rot}} = \delta_a F_z^{(a)} - \delta_b F_z^{(b)} + \Omega_{\text{rf}} [(F_+^{(a)} + F_-^{(a)}) - (F_+^{(b)} + F_-^{(b)})], \quad (\text{A22})$$

where $\delta_a = \omega_a - \omega_{\text{rf}}$ and $\delta_b = \omega_b - \omega_{\text{rf}}$ are the detunings of the Larmor frequency ω_a and ω_b with respect to the rf frequency ω_{rf} .

Consequently, the total Hamiltonian H_{eff} of our system is the sum of the unperturbed Hamiltonian $\tilde{H}_0 = -\Delta \sum_{M_{F_b}} |F_b M_{F_b}\rangle \langle F_b M_{F_b}|$, where $\Delta = 9193$ MHz is the hyperfine detuning of two ground states, the light-atom-interaction Hamiltonian \tilde{H}_L , and the magnetic-field-atom-interaction Hamiltonian \tilde{H}_B^{rot} ,

$$H_{\text{eff}} = \tilde{H}_0 + \Delta_{\text{AC}} (F_z^{(b)})^2 + \delta_a F_z^{(a)} - \delta_b F_z^{(b)} + \Omega_{\text{rf}} [(F_+^{(a)} + F_-^{(a)}) - (F_+^{(b)} + F_-^{(b)})]. \quad (\text{A23})$$

One is given directly in the main text in Eq. (5).

APPENDIX B: EVOLUTION EQUATIONS OF ATOMIC MULTIPOLE MOMENTS

Under the frame rotating of the rf frequency to the system of atomic multipole moments, the slow evolution of $m_{k,q}^b$ for $F_b = 3$ level is given by

with the same rank k and component q , which causes the total atomic population, orientation, and alignment to be

transferred between the two ground-state levels. However, due to the $F_a = 4$ and $F_b = 3$ states present opposite Larmor precession directions, the process of frame rotating of the rf frequency ω_{rf} to the system is equivalent to doing the opposite transform: $\tilde{m}_{k,q}^b = m_{k,q}^b e^{qi\omega_{\text{rf}}t}$ for $F_b = 3$ level while $\tilde{m}_{k,q}^a = m_{k,q}^a e^{-qi\omega_{\text{rf}}t}$ for $F_a = 4$ level. Therefore, the coupling between the transverse multipole moments $m_{k,q}^b (q \neq 0)$ and $m_{k,q}^a (q \neq 0)$ contains the fast rf-oscillating term, shown in the last term of Eqs. (B1b), (B1d), and (B1e).

In our system, the value of the rf frequency is tuned to (22.0–22.8) kHz, which is much larger than the SEC

relaxation coefficient $c_k^{\text{se}} \approx 10$ Hz. In the case of $\omega_{\text{rf}} \gg c_k^{\text{se}}$, the secular approximation can be adopted, i.e., the fast rf-oscillating term [the last term of Eqs. (B1b), (B1d), and (B1e)] can be ignored under the long-time approximation. Consequently, the coupling between the transverse multipole moments $m_{k,q}^b (q \neq 0)$ and $m_{k,q}^a (q \neq 0)$ caused by SEC can be ignored, then Eq. (B1) can be simplified to Eq. (9) in Sec. IID. In Eq. (9), only the coupling between the longitudinal multipole moment $m_{k,0}^b$ and that of $m_{k,0}^a$ is shown.

Similarly, the evolution equations of atomic multipole moments $m_{k,q}^a$ for $F_a = 4$ level are obtained and shown in Eq. (10) in Sec. IID.

APPENDIX C: LASER-INDUCED EQUIVALENT RELAXATION RATES

In the calculations of the density-matrix theory, the laser-induced equivalent relaxation process $\mathcal{L}_L \tilde{\rho}$ is described by Eq. (A13). Substituting Eq. (A13) into Eq. (8) enables one to calculate the evolution of the atomic multipole moments due to the combined action of the optical pumping and spontaneous emission. The laser-induced equivalent relaxation rates of atomic multipole moments m_{kq}^b and m_{kq}^a are written by p_{kq}^b and p_{kq}^a , respectively. The detailed expressions are given by

$$\begin{aligned}
 p_{10}^a &= \frac{\Omega_L^2}{64} \sqrt{\frac{7}{15}} \left(\frac{35\Gamma}{\Gamma^2 + 4\Delta_3^2} + \frac{19\Gamma}{\Gamma^2 + 4\Delta_4^2} \right), \\
 p_{11}^a &= \frac{\Omega_L^2}{32} \sqrt{\frac{7}{15}} \left(\frac{5\Gamma}{\Gamma^2 + 4\Delta_3^2} + \frac{19\Gamma}{\Gamma^2 + 4\Delta_4^2} \right), \\
 p_{20}^a &= \frac{5\Omega_L^2}{4032} \sqrt{\frac{11}{3}} \left(\frac{117\Gamma}{\Gamma^2 + 4\Delta_3^2} + \frac{85\Gamma}{\Gamma^2 + 4\Delta_4^2} \right), \\
 p_{21}^a &= \frac{5\Omega_L^2}{672} \sqrt{\frac{11}{3}} \left(\frac{15\Gamma}{\Gamma^2 + 4\Delta_3^2} + \frac{17\Gamma}{\Gamma^2 + 4\Delta_4^2} \right), \\
 p_{22}^a &= \frac{5\Omega_L^2}{448} \sqrt{\frac{11}{3}} \left(\frac{\Gamma}{\Gamma^2 + 4\Delta_3^2} + \frac{17\Gamma}{\Gamma^2 + 4\Delta_4^2} \right), \\
 p_{00}^b &= \frac{\Omega_L^2}{12} \left(\frac{3\Gamma}{\Gamma^2 + 4\Delta_3^2} + \frac{5\Gamma}{\Gamma^2 + 4\Delta_4^2} \right), \\
 p_{10}^b &= \frac{\Omega_L^2}{4032} \left(\frac{512\Gamma}{\Gamma^2 + 4\Delta_2^2} + \frac{2205\Gamma}{\Gamma^2 + 4\Delta_3^2} + \frac{1485\Gamma}{\Gamma^2 + 4\Delta_4^2} \right), \\
 p_{11}^b &= \frac{\Omega_L^2}{288} \left(\frac{64\Gamma}{\Gamma^2 + 4\Delta_2^2} + \frac{81\Gamma}{\Gamma^2 + 4\Delta_3^2} + \frac{135\Gamma}{\Gamma^2 + 4\Delta_4^2} \right), \\
 p_{20}^b &= \frac{\Omega_L^2}{197568} \left(\frac{36864\Gamma}{\Gamma^2 + 4\Delta_2^2} + \frac{120393\Gamma}{\Gamma^2 + 4\Delta_3^2} + \frac{88265\Gamma}{\Gamma^2 + 4\Delta_4^2} \right), \\
 p_{21}^b &= \frac{\Omega_L^2}{32928} \left(\frac{8000\Gamma}{\Gamma^2 + 4\Delta_2^2} + \frac{19551\Gamma}{\Gamma^2 + 4\Delta_3^2} + \frac{15105\Gamma}{\Gamma^2 + 4\Delta_4^2} \right), \\
 p_{22}^b &= \frac{\Omega_L^2}{65856} \left(\frac{27136\Gamma}{\Gamma^2 + 4\Delta_2^2} + \frac{36015\Gamma}{\Gamma^2 + 4\Delta_3^2} + \frac{32575\Gamma}{\Gamma^2 + 4\Delta_4^2} \right). \tag{C1}
 \end{aligned}$$

In Eq. (C1), Ω_L is the reduced Rabi frequency of the laser field, Γ is the total spontaneous emission relaxation rate from excited state F' to the two hyperfine ground states, and the detuning $\Delta_{F'}$ is the frequency difference between the atomic $F_b = 3 \rightarrow F' (F' = 2, 3, 4)$ transition and the laser frequency. The laser-induced equivalent relaxation rates $p_{1q}^b (q = 0, 1)$ and $p_{2q}^b (q = 0, 1, 2)$ relate to atomic orientation and alignment in the $F_b = 3$ state. Similarly, $p_{1q}^a (q = 0, 1)$ and $p_{2q}^a (q = 0, 1, 2)$ correspond to atomic orientation and alignment in the $F_a = 4$ state.

[1] A. K. Zvezdin and V. A. Kotov, *Modern Magneto-optics and Magneto-optical Materials* (1997).

[2] D. Budker, W. Gawlik, D. F. Kimball, S. M. Rochester, V. V. Yashchuk, and A. Weis, Resonant nonlinear

- magneto-optical effects in atoms, *Rev. Mod. Phys.* **74**, 1153 (2002).
- [3] M. Auzinsh, D. Budker, and S. Rochester, *Optically Polarized Atoms: Understanding Light-Atom Interactions* (Oxford University Press, Oxford, 2010).
- [4] M. Faraday, Experimental researches in electricity.nineteenth series, London, Edinburgh, Dublin Philos. Mag. J. Sci. **28**, 294 (1846).
- [5] W. Voigt, Ueber das elektrische Analogon des Zeemaneffectes, *Ann. Phys.* **309**, 197 (1901).
- [6] A. K. Patnaik and G. Agarwal, Laser field induced birefringence and enhancement of magneto-optical rotation, *Opt. Commun.* **179**, 97 (2000).
- [7] S. Li, B. Wang, X. Yang, Y. Han, H. Wang, M. Xiao, and K. C. Peng, Controlled polarization rotation of an optical field in multi-Zeeman-sublevel atoms, *Phys. Rev. A* **74**, 033821 (2006).
- [8] P. Siddons, C. S. Adams, and I. G. Hughes, Optical control of Faraday rotation in hot Rb vapor, *Phys. Rev. A* **81**, 043838 (2010).
- [9] A. Morteza pour, M. Abad, and M. Mahmoudi, Magneto-optical rotation in a GaAs quantum well waveguide, *J. Opt. Soc. Am. B* **32**, 1338 (2015).
- [10] S. A. Mousavi, E. Plum, J. Shi, and N. I. Zheludev, Coherent control of optical polarization effects in metamaterials, *Sci. Rep.* **5**, 8977 (2015).
- [11] I. Crassee, J. Levallois, A. L. Walter, M. Ostler, A. Bostwick, E. Rotenberg, T. Seyller, V. Dirck, and A. B. Kuzmenko, Giant Faraday rotation in single- and multilayer graphene, *Nat. Phys.* **7**, 48 (2011).
- [12] J. C. Martinez, M. Jalil, and S. G. Tan, Optical faraday rotation with graphene, *J. Appl. Phys.* **113**, 204302 (2013).
- [13] A. Morteza pour, M. Abad, and M. A. Borji, Magneto-optical rotation in the diamond nitrogen-vacancy center, *Laser Phys. Lett.* **13**, 055202 (2016).
- [14] D. F. Kimball, D. Budker, D. S. English, C.-H. Li, A.-T. Nguyen, S. M. Rochester, A. Sushkov, V. V. Yashchuk, and M. Zolotarev, Progress towards fundamental symmetry tests with nonlinear optical rotation, *AIP Conf. Proc.* **596**, 84 (2001).
- [15] S. Knappe, P. Schwindt, V. Shah, L. Hollberg, and J. Moreland, A chip-scale atomic clock based on ^{87}Rb with improved frequency stability, *Opt. Express* **13**, 1249 (2005).
- [16] M. Fleischhauer, A. B. Matsko, and M. O. Scully, Quantum limit of optical magnetometry in the presence of ac Stark shifts, *Phys. Rev. A* **62**, 013808 (2000).
- [17] D. Budker, D. F. Kimball, S. M. Rochester, V. V. Yashchuk, and M. Zolotarev, Sensitive magnetometry based on nonlinear magneto-optical rotation, *Phys. Rev. A* **62**, 043403 (2000).
- [18] I. Novikova and G. R. Welch, Magnetometry in dense coherent media, *J. Mod. Opt.* **49**, 349 (2002).
- [19] G. A. Smith, S. Chaudhury, A. Silberfarb, I. H. Deutsch, and P. S. Jessen, Continuous Weak Measurement and Nonlinear Dynamics in a Cold Spin Ensemble, *Phys. Rev. Lett.* **93**, 163602 (2004).
- [20] M. C. Kuntz, R. C. Hilborn, and A. M. Spencer, Dynamic Stark shift and alignment-to-orientation conversion, *Phys. Rev. A* **65**, 023411 (2002).
- [21] I. M. Savukov and M. V. Romalis, Effects of spin-exchange collisions in a high-density alkali-metal vapor in low magnetic fields, *Phys. Rev. A* **71**, 023405 (2005).
- [22] U. Fano, Precession equation of a spinning particle in nonuniform fields, *Phys. Rev.* **133**, B828 (1964).
- [23] T. Manabe, T. Yabuzaki, and T. Ogawa, Observation of Collisional Transfer from Alignment to Orientation of Atoms Excited by a Single-Mode Laser, *Phys. Rev. Lett.* **46**, 637 (1981).
- [24] M. Krainska-Miszczak, Alignment and orientation by optical pumping with pi polarised light, *J. Phys. B* **12**, 555 (1979).
- [25] R. C. Hilborn, L. R. Hunter, K. Johnson, S. K. Peck, A. Spencer, and J. Watson, Atomic barium and cesium alignment-to-orientation conversion in external electric and magnetic fields, *Phys. Rev. A* **50**, 2467 (1994).
- [26] I. Novikova, A. B. Matsko, V. A. Sautenkov, V. L. Velichansky, G. R. Welch, and M. O. Scully, Ac-Stark shifts in the nonlinear faraday effect, *Opt. Lett.* **25**, 1651 (2000).
- [27] J. Alnis and M. Auzinsh, Angular-momentum spatial distribution symmetry breaking in Rb by an external magnetic field, *Phys. Rev. A* **63**, 023407 (2001).
- [28] D. Budker, D. F. Kimball, S. M. Rochester, and V. V. Yashchuk, Nonlinear Magneto-optical Rotation via Alignment-to-Orientation Conversion, *Phys. Rev. Lett.* **85**, 2088 (2000).
- [29] D. Budker, D. F. Kimball, S. M. Rochester, and J. T., Alignment-to-orientation conversion and nuclear quadrupole resonance, *Chem. Phys. Lett.* (2003).
- [30] S. M. Rochester, M. P. Ledbetter, T. Zigdon, A. D. Wilson-Gordon, and D. Budker, Orientation-to-alignment conversion and spin squeezing, *Phys. Rev. A* **85**, 022125 (2012).
- [31] P. Bevington, R. Gartman, and W. Chalupczak, Generation of atomic spin orientation with a linearly polarized beam in room-temperature alkali-metal vapor, *Phys. Rev. A* **101**, 013436 (2020).
- [32] W. Chalupczak and P. Josephs-Franks, Alkali-Metal Spin Maser, *Phys. Rev. Lett.* **115**, 033004 (2015).
- [33] K. Blum, *Density Matrix Theory and Applications* (Plenum, New York, 1978).
- [34] S. Appelt, A. B. Baranga, C. J. Erickson, M. V. Romalis, A. R. Young, and W. Happer, Theory of spin-exchange optical pumping of ^3He and ^{129}Xe , *Phys. Rev. A* **58**, 1412 (1998).
- [35] T. Zigdon, A. D. Wilson-Gordon, Wilson-Gordon, S. Guttikonda, and E. J. Bahr, Nonlinear magneto-optical rotation in the presence of a radio-frequency field, *Opt. Express* (2010).
- [36] Y. P. Malakyan, S. M. Rochester, D. Budker, D. F. Kimball, and V. V. Yashchuk, Nonlinear magneto-optical rotation of frequency-modulated light resonant with a low- j transition, *Phys. Rev. A* **69**, 013817 (2004).
- [37] G. Bevilacqua, E. Breschi, and A. Weis, Steady-state solutions for atomic multipole moments in an arbitrarily oriented static magnetic field, *Phys. Rev. A* **89**, 033406 (2014).
- [38] A. Weis, G. Bison, and A. S. Pazgalev, Theory of double resonance magnetometers based on atomic alignment, *Phys. Rev. A* **74**, 033401 (2006).
- [39] P. L. Qi, X. X. Geng, G. Q. Yang, G. M. Huang, and G. X. Li, Theory of double-resonance alignment magnetometers based on atomic high-order multipole moments using effective master equations, *J. Opt. Soc. Am. B* **37**, 3303 (2020).